Spatial constraints control cell proliferation in tissues

Sebastian J. Streichan[a,b,1,2], Christian R. Hoerner[b,c,1], Tatjana Schneidt[b], Daniela Holzer[b], and Lars Hufnagel[b,2]

[a]Kavli Institute for Theoretical Physics, University of California, Santa Barbara, CA 93106; [b]Cell Biology and Biophysics Unit, European Molecular Biology Laboratory, 69117 Heidelberg, Germany; and [c]Department of Biology, Stanford University, Stanford, CA 94305

Edited by Robert H. Austin, Princeton University, Princeton, NJ, and approved February 28, 2014 (received for review December 11, 2013)

Control of cell proliferation is a fundamental aspect of tissue formation in development and regeneration. Cells experience various spatial and mechanical constraints depending on their environmental context in the body, but we do not fully understand if and how such constraints influence cell cycle progression and thereby proliferation patterns in tissues. Here, we study the impact of mechanical manipulations on the cell cycle of individual cells within a mammalian model epithelium. By monitoring the response to experimentally applied forces, we find a checkpoint at the G1–S boundary that, in response to spatial constraints, controls cell cycle progression. This checkpoint prevents cells from entering S phase if the available space remains below a characteristic threshold because of crowding. Stretching the tissue results in fast cell cycle reactivation, whereas compression rapidly leads to cell cycle arrest. Our kinetic analysis of this response shows that cells have no memory of past constraints and allows us to formulate a biophysical model that predicts tissue growth in response to changes in spatial constraints in the environment. This characteristic biomechanical cell cycle response likely serves as a fundamental control mechanism to maintain tissue integrity and to ensure control of tissue growth during development and regeneration.

cell cycle regulation | mechanical feedback | quantitative biology | size checkpoint | G1-S transition

Control of cell division during tissue formation is a major regulatory principle of tissue and organ formation, size determination, tissue regeneration, and tumorigenesis (1, 2). Unicellular lower eukaryotic organisms, such as the budding yeast *Saccharomyces cerevisiae*, link cell division to cell growth through a size checkpoint during late G1 phase (3–5). This size checkpoint, termed "start" in yeast, is believed to ensure that only cells that have reached a characteristic size enter the cell cycle; it is therefore critical for cell size homeostasis. However, it is not known how cells monitor their own size. The situation is even less clear in mammalian cells. Although early studies in cultured cells argued for a size checkpoint similar to that of yeast (6), more recent reports instead proposed the growth rate as a trigger for cell division (7–11). In this view, reaching a characteristic growth rate rather than a characteristic size triggers entry into S phase. The molecular basis of neither model is well understood.

The body of animals largely comprises cohesive tissues in which cells are not in isolation, but are coupled mechanically through their cell–cell and cell–substrate contacts (12–14). Spatial constraints from crowding, i.e., limitations on available space due to the presence of neighboring cells, impose constraints on cell functions, such as cell proliferation. Thus, the regulation of spatial constraints in tissues possibly represents a tissue-level feedback on the cell cycle regulation of individual cells. Indeed, experimental and theoretical studies have proposed that physical parameters, such as cell geometry or local tissue mechanics, regulate cell division (15–20). However, most of the evidence so far is based on correlation, and it remains unclear whether mechanical constraints control cell cycle progression in growing tissues and at what stage of the cell cycle this regulation may act.

To address this question, we have combined live imaging of the cell cycle state of individual cells over time in a model epithelium with experimental perturbation of its spatial constraints. We either acutely removed a barrier to release spatial constraints at the edge of the model epithelium or performed mechanical stretching or compression of the tissue substrate to manipulate spatial constraints directly within the model tissue, a method previously applied only to end point assays (21–26). We show that the proliferation rate in tissues is controlled by a mechanosensitive cell cycle checkpoint that monitors the space available to the cell at the G1–S interface. Using mathematical modeling, we can predict the tissue response to changes in spatial constraints and validate the prediction of the model that cell division is required for sustained invasion of a tissue into newly colonized space.

Results

Spatial Constraints Regulate Cell Cycle Progression During Tissue Expansion. To probe mechanical control of cell cycle progression in growing tissues, we decided to introduce rapid and temporally controlled alterations of spatial constraints in a tissue colonization assay: We grew an epithelial model tissue consisting of contact-inhibited, fully polarized Madin–Darby canine kidney-2 (MDCK-2) cells against a removable barrier (Fig. 1*A*) (26, 27). To monitor cell cycle dynamics, we used a fluorescent ubiquitination-based cell cycle indicator (Fucci; Fig. 1*A*, Fig. S1, and Movie S1) (28). After barrier removal, the tissue rapidly invaded the available space, and after a slight delay, cells behind the initial barrier also reactivated their cell cycle by entering S phase (Fig. 1 *C*–*F* and Movie S2). This was accompanied by a noted increase in the space covered by individual cells, i.e., the cross-sectional cell area (henceforth called "cell area"), from the edge of the tissue reaching into the tissue (Fig. 1 *C′*–*F′* and Movie S2). Interestingly, cells entered S phase in all regions of increased cell area up to several hundred micrometers behind the initial barrier, whereas cells even further behind

Significance

Spatiotemporal coordination of cell growth underlies tissue development and disease. Mechanical feedback between cells has been proposed as a regulatory mechanism for growth control both in vivo and in cultured cells undergoing contact inhibition of proliferation. Evidence beyond theoretical and correlative observations falls short. In this study, we probe the impact of mechanical tissue perturbations on cell cycle progression by monitoring cell cycle dynamics of cells in tissues subject to acute changes in boundary conditions, as well as tissue stretching and compression. Taken together, we conclude that the ability of tissues to support cell cycle progression adapts to the available space through a memory-free control mechanism, which may coordinate proliferation patterns to maintain tissue homeostasis.

Author contributions: S.J.S. and L.H. designed research; S.J.S., C.R.H., and T.S. performed research; S.J.S. and D.H. contributed new reagents/analytic tools; S.J.S. and C.R.H. analyzed data; and S.J.S., C.R.H., and L.H. wrote the paper.

The authors declare no conflict of interest.

This article is a PNAS Direct Submission.

[1]S.J.S. and C.R.H. contributed equally to this work.

[2]To whom correspondence may be addressed. E-mail: streicha@kitp.ucsb.edu or hufnagel@embl.de.

This article contains supporting information online at www.pnas.org/lookup/suppl/doi:10.1073/pnas.1323016111/-/DCSupplemental.

www.pnas.org/cgi/doi/10.1073/pnas.1323016111

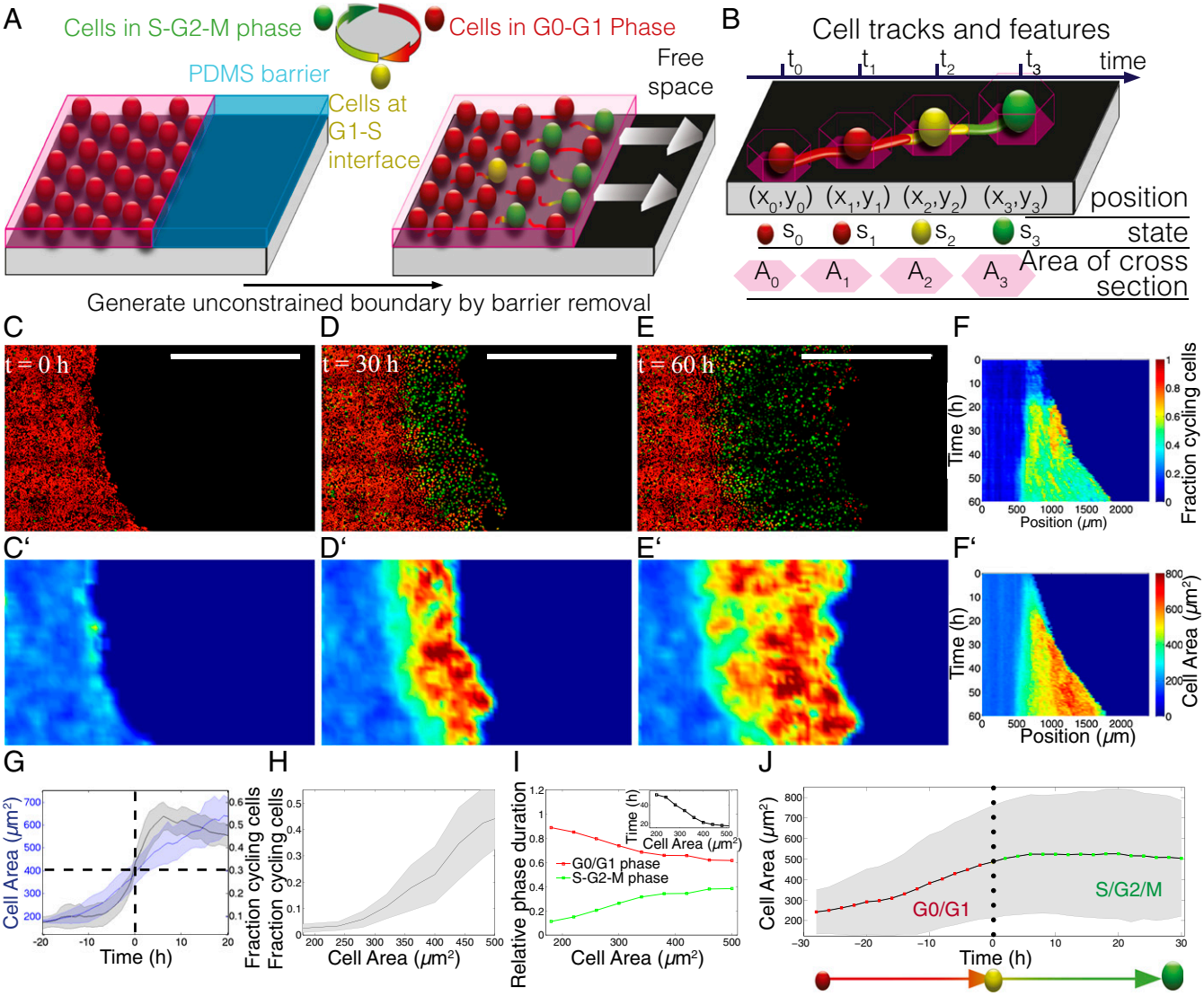

Fig. 1. Cellular area correlates with cell cycle progression during tissue invasion. (*A*) Fucci cell cycle marker in tissue invasion assay. (*Left*) Cells in G0–G1 phase constrained by a polydimethylsiloxane (PDMS) barrier. (*Right*) Shortly before imaging, the boundary is removed, generating free space available to the tissue. (*B*) Single cell track over time and extraction of features at each time point: position, cell cycle state, and cell area. (*C*) MDCK Fucci cells in tissue colonization assay. Representative images of the progressing tissue are shown 0 h, 30 h, and 60 h (*C*–*E*) after barrier removal. The tissue invades the free space, and cells progress in the cell cycle. Scale bars: 500 μm. (*C′*–*F′*) Average cell area at the same time points as in *C*–*E*, color-coded as in *F′*. (*D*) As *C*. (*D′*) As *C′*. (*E*) As *C*. (*E′*) As *C′*. (*F*) Kymograph showing temporal evolution of FCC (color coded). (*F′*) As *F* for cell area. (*G*) Cell area (blue) and FCC (gray) plotted against time aligned to the first occurrence of 30% cycling cells (indicated by the horizontal black dashed line) in a segment behind the leading edge ($t = 0$, vertical black dashed line). (*H*) Mean FCC plotted against cell area for the whole course of the experiment. Error bar: SD. (*I*) Duration of G0–G1 (red) phase or S–G2–M (green) phase relative to total cell cycle duration, respectively, plotted against cell area. (*Inset*) Total cell cycle duration as a function of cell area. (*J*) Mean cell area for each time point during cell cycle progression. Time is aligned to the G1–S transition ($t = 0$ h, black dotted line). Color-coding below indicates Fucci marker (guide for the eye). Error bars: SD.

remained at high density and did not exhibit signs of increased proliferation (Fig. 1 *C*–*F*).

Quantification of the changes in the mean cell areas and cell cycle states revealed that the increase in cell area preceded an increase in the fraction of cycling cells (FCC) (Fig. 1 *F* and *G*, Fig. S2, and *SI Materials and Methods*). Interestingly, the FCC sharply increased after the cell area exceeded a threshold of about 350 μm^2 (Fig. 1*H* and Fig. S3). This proliferation behavior suggests that the probability of cell cycle progression for individual cells increases with cell area and that proliferation is not triggered by the release of growth factors from cells at the leading edge.

Analysis of trajectories of individual cells over time indeed revealed that the cell area gradually increased in G1 phase until it reached a critical value of 470 ($\pm$270) μm^2 at the onset of S phase (Fig. 1 *B* and *J*). This is consistent with the marked increase in the FCC at similar cell areas. Statistical analysis of the single cell trajectories furthermore showed that smaller cells had an increased total cell cycle duration caused largely by a prolonged G1 phase (Fig. 1*I* and Fig. S2). Thus, smaller cells apparently require a longer time of growth in G1 before they can proceed to S phase.

Together, these results suggest that cells in an invasive tissue rapidly adapt to the release of spatial constraints by first increasing their size until they pass a critical threshold required for S phase entry. To rule out that removal of the barrier induced biochemical signals by wounding the directly attached cells rather than changing the mechanical constraints of the tissue

DEVELOPMENTAL BIOLOGY

(29), we next developed a device that allowed us to manipulate the epithelial tissue purely mechanically.

Externally Applied Forces Regulate Cell Cycle Progression. We designed and constructed a mechanical manipulation device that allowed us to stretch or compress the epithelial tissue grown on an elastic substrate during live imaging (Fig. 2 *A*–*C*). Control experiments on unperturbed substrates confirmed that cells showed a similar correlation between cell area and FCC as on glass, and the FCC decreased with smaller areas (Fig. 2*F* and Fig. S4). Only the steady-state cell area was slightly smaller because of differences in the substrate material.

We next set out to systematically study the cellular response of a contact-inhibited tissue immediately after stretching until a new steady state was reached. Rapid extension of the substrate to twice its initial length led to an immediate increase in cell area and correspondingly to a lower cell density while leaving cell–cell junctions intact (Fig. S4 and Movie S3). With a delay of approximately 8 h, we observed a significant increase in the FCC within 20 h and a return to levels similar to those before stretching within 50 h (Fig. 2*D*). This return was accompanied by an increase in cell density and a decrease in cell area to its initial levels. Stretching tissues consisting of mouse inner medullary collecting duct-3 (mIMCD-3) cells resulted in similar observations, suggesting that this is a general response of mammalian epithelia (Movie S4).

We then analyzed the cellular response of the contact-inhibited epithelium to varying degrees of stretching. We found that the epithelial monolayer remained intact when stretching up to 2.5-fold (Fig. S4). Less than 2.5-fold stretching of the substrate resulted in an increase in cell area, and in response, the FCC always increased. The extent of this response correlated with the fold of stretching: the more the substrate was stretched, the higher was the increase in cell area and in the FCC (Fig. 2*G*). Thus, the fraction of cells committed to the cell cycle was sensitive to the available space after stretching. This proliferative phase lasted until the tissue returned to contact inhibition and to cell areas and a corresponding cell density that were similar to those before stretching (Fig. 2*G*).

Then we compared this relationship between the FCC and cell area during the proliferative phase of a stretched tissue with the unperturbed control, as characterized above (Fig. 2*F*). Interestingly, the fraction of cycling cells followed the same relationship to cell area as the unstretched reference tissue, and this relationship was maintained independent of the fold stretching (Fig. 2*G*). Moreover, the FCC dropped in the same fashion as the unperturbed proliferating control. In other words, the FCC at each time point could be predicted from the current cell area, regardless of whether unperturbed proliferating cells underwent size-reductive divisions or previously contact-inhibited cells went through a proliferative phase after stretching (Fig. 2*G*).

We then tested whether this relationship between cell area and FCC also controls cell cycle progression when cell areas become actively reduced (instead of increased, as above). To this end, we cultured confluent cells at low density on a prestretched substrate. We then tested whether we could decrease the FCC when we reduced cell area by relaxing the substrate, thereby compressing the tissue. The reduction in cell area due to tissue compression resulted in a reduction in the FCC within 20 h (Fig. 2*E*, Fig. S4, and Movie S5). As a consequence of compression, the FCC dropped to levels corresponding to unperturbed control tissues with the same cell area. This effect was consistent for varying initial cell areas and different extents of compression (Fig. S4*G*).

In summary, cell proliferation toward contact inhibition of proliferation and in response to the release of spatial constraints both show the same trend: tissues adapt to changes in the available space for cell proliferation by up- or down-regulating the FCC, respectively, according to the available space. Taken together, this suggests that spatial constraints play an instructive role in cell cycle progression.

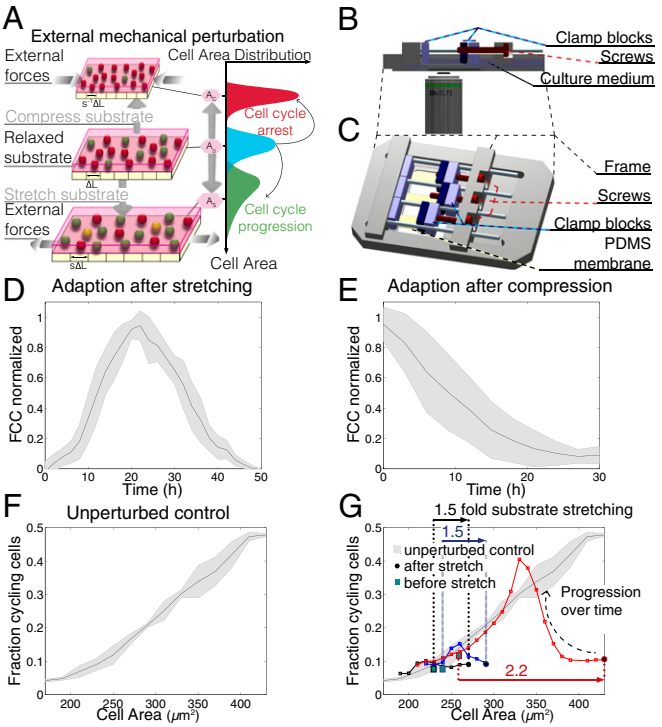

Fig. 2. Cell cycle dynamically adapts to biomechanical tissue manipulations. (*A*) Mechanical perturbation assay. (*Left*, *Middle*) Cells on relaxed elastic substrate. Substrate compression or stretching reduces or increases cell area, respectively. (*Right*) Response of cell area distribution and expected cell cycle dynamics to perturbation. (*B*) Stretcher setup; side view with objective from below. A PDMS membrane (yellow) is clamped between the frame (gray) and a fixed block (light blue) and on the other side between two mobile blocks (light and dark blue), allowing the length of the PDMS membrane to be adjusted. (*C*) Top view of *B*. (*D*) Fraction of cycling cells against area after stretching at $t = 0$ h. The number 1 corresponds to the maximum of the FCC and 0 to the FCC before stretching. Error bars: SD. (*E*) Fraction of cycling cells against area after compression at $t = 0$ h. The number 1 corresponds to the FCC before compression and 0 to the minimum FCC. Error bars: SD. (*F*) Unperturbed control FCC against area for tissues growing toward contact inhibition of proliferation. (*G*) Fraction of cycling cells vs. cell area for stretched tissues. Graph color codes for different experiments. The fold stretching of the substrate is indicated by color-coded arrows, which connect the initial FCC (blue ■) to the FCC after stretching (●). Gray background shading indicates control curve (*F*); the black dashed arrow indicates temporal progression of the FCC and cell area after stretching.

Cell Cycle Reactivation Has No Memory of Past Spatial Constraints and Requires MAP Kinase Signaling. The rapid adaption of the FCC and, therefore, cell cycle progression after mechanical perturbations (tissue stretching or compression) suggests that cells have no memory of their previous spatial constrained state or, in other words, that the control mechanism displays no hysteresis. Interestingly, the reduction in cycling cells after compression of tissues grown on a prestretched membrane was the same as for tissues grown on a relaxed membrane, which first was stretched and then compressed only 24 h after stretching (Fig. S4*H*), indicating an absence of memory. As these responses occurred on a time scale shorter than the average cell cycle duration, our data strongly suggest a hysteresis-free regulatory mechanism.

Our data so far show that spatial constraints control entry into S phase and suggest the existence of a "spatial checkpoint" at the G1–S boundary. Cells therefore should be able to monitor the

available space to control cell cycle progression. The ability to induce S phase entry by tissue stretching provided us with an assay to investigate the molecular mechanism of the spatial checkpoint. Inhibition of the MAPK/ERK kinase (MEK) with a small molecule inhibitor prevented cells in a stretched tissue from entering S phase (Fig. 3*A*). Washout of the inhibitor while the tissue was maintained in the stretched state resulted in a strong increase in the FCC to levels similar to those of an untreated control epithelium under the same conditions of stretching (Fig. 3*B*, Fig. S4, and Movie S6). This response was specific to the mechanical perturbation, as inhibitor washout from a stretched tissue with simultaneous tissue relaxation showed no increase in the FCC (Fig. 3*C* and Movie S7), showing that the tissue has no memory of past spatial constraints.

Cell Cycle Reactivation Drives Sustained Epithelial Colonization. To predict the behavior of an invading epithelium, we formulated a phenomenological biophysical model of cell cycle regulation in an epithelial tissue based on our quantitative data. We modeled the cell cycle to include a G phase (reflecting G1 phase) and an S phase (reflecting G2, S, and M phase), similar to ref. 30; the probability of S-phase entry in G is area dependent whereas the probability of dividing during S is not (Fig. S5*C*). To simulate the boundary release experiment, we coupled our cell cycle model to the biophysical vertex model (20, 31, 32) (Fig. 4*B*, Fig. S5, and *SI Materials and Methods* for more details). Briefly, the vertex model describes tissues as a lattice of cells as central units and determines the configuration of cells in the lattice through minimization of an energy that reflects phenomenological observables, such as a preferred cell perimeter, cell area, or cell–substrate attachment. To obtain initial conditions reflecting the observations of the experiments, we initialized lattices with boundary conditions and comprising only cells with subcritical area, resulting in a vanishing S-phase entrance probability (Fig. 4*B*). At the beginning of the simulations, we released the boundary conditions and assumed a maximum outward-directed crawling velocity v_{max} for the boundary cells (Fig. 4*B*).

We fitted this model to the experimentally obtained data, which resulted in simulations recapitulating key aspects of the tissue behavior. These included the velocity changes of the invading tissue boundary and the cell cycle reactivation, not only at the invading front but also several cell layers behind it (Fig. S5 *A*, *B*, *F*, and *G*). Using this model, we could assess the importance of cell cycle reentry for sustained tissue invasion of free space. In contrast to previous reports (27), in which collective migration was found to be independent from proliferation, it predicts that tissue invasion without tissue proliferation would stall rapidly after an initial wave of movement and therefore would not be sustainable (Fig. 4 *C* and *D*). The model furthermore predicts that even a stalled invading tissue can resume colonization if proliferation can be reactivated, which is accompanied by cell cycle reentry of cells in a spatial pattern that immediately expands far behind the leading edge (Fig. 4 *C* and *D*).

To verify this prediction of our model, we inhibited cell cycle progression using the MEK inhibitor in the boundary release assay before barrier removal (Fig. 4*A*). Initially, cells invaded the free space with a velocity comparable to that of control tissues, despite being stalled in the cell cycle (Fig. 4 *E* and *F*, Fig. S6 *E* and *F*, and Movie S8). However, as our model predicted, the leading edge of the tissue slowed rapidly again after only approximately 10 h of movement (Fig. 4 *E* and *F*), showing that cell proliferation is required for sustained tissue advance into free space. Release of the cell cycle block caused rapid cell cycle reentry of cells up to many rows behind the leading edge (Fig. 4*E* and Fig. S6*E*) and restored the invasive movement of the tissue, whose boundary accelerated until it reached a velocity comparable to that of controls (Fig. S5*B* and Fig. 4*F*). This shows that cell proliferation is sufficient to sustain tissue colonization if space is available. Notably, we found the same relationship between the increased cell area and the FCC as in the untreated boundary release assay (Fig. S6*D*). Both observations are in excellent agreement with the predictions of our tissue invasion model and demonstrate that a simple mechanism of an elastic tissue composed of cells with a hysteresis-free spatial checkpoint for cell cycle reentry explains all our observations.

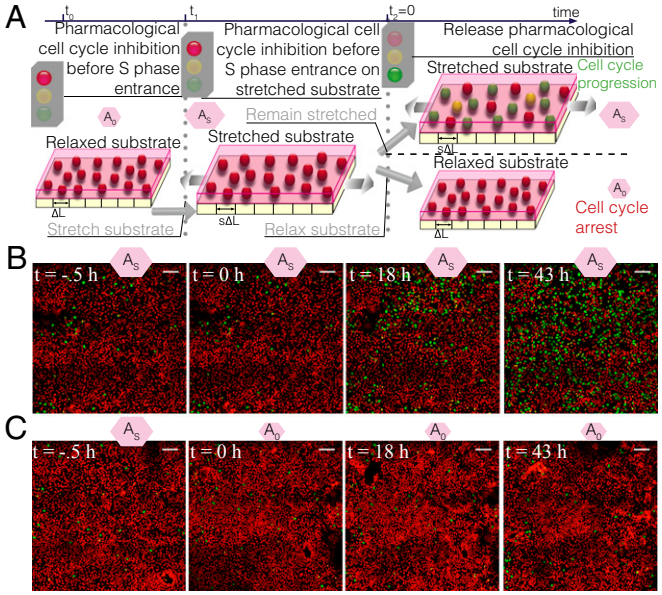

Fig. 3. Dynamics of cell cycle activation reveal a memory-free biomechanical cell cycle checkpoint for available space. (*A*) Schematic of the tissue stretch assay. Cell cycle is blocked with a MEK inhibitor (added at t_0) before S-phase entrance and the substrate is stretched (at t_1). Two scenarios are tested upon release of the cell cycle block (at t_2): The tissue remains stretched (*Upper*) or becomes compressed right after release of the cell cycle block (*Lower*). (*B*) Representative time series of a tissue comprising MDCK Fucci cells treated with a MEK inhibitor before substrate stretching. $t = 0$ h corresponds to the time of MEK inhibitor washout. Scale bar: 100 μm. (*C*) Representative time series of a tissue comprising MDCK Fucci cells treated with a MEK inhibitor before substrate stretching. $t = 0$ h corresponds to the time of MEK inhibitor washout and parallel relaxation of the substrate to its length before stretching. Scale bar: 100 μm.

Discussion

In this study, we identified spatial constraints as a regulator of cell cycle progression in growing tissues via a spatial checkpoint at the G1–S transition. Furthermore, we demonstrated that in the observed ranges, cross-sectional cell area is a characteristic measure for the activation state of this checkpoint. Such a checkpoint in tissues is analogous to findings in yeast, in which a size checkpoint controls the duration of G1 phase (4). However, it is in contrast to mechanisms identified in single mammalian cells, in which it was suggested that the cellular growth rate determines cell cycle progression (11). The relative importance of environmental aspects required for cell cycle progression changes for cells in crowded tissues: Although for single cells it may be sufficient to integrate an abundance of nutrients by, e.g., the growth rate, tissues also need to incorporate cell–cell and cell–substrate interactions, which is reflected by the area in which cells spread. These differences might result from mechanical coupling between cells in tissues via their adhesive cell–cell contacts, which do not exist in single cells.

The fact that we found that the critical cell area for S-phase entry depends on the tissue substrate emphasizes the importance of matrix properties (e.g., stiffness) and suggests a non–cell-autonomous component in the sensing of spatial constraints

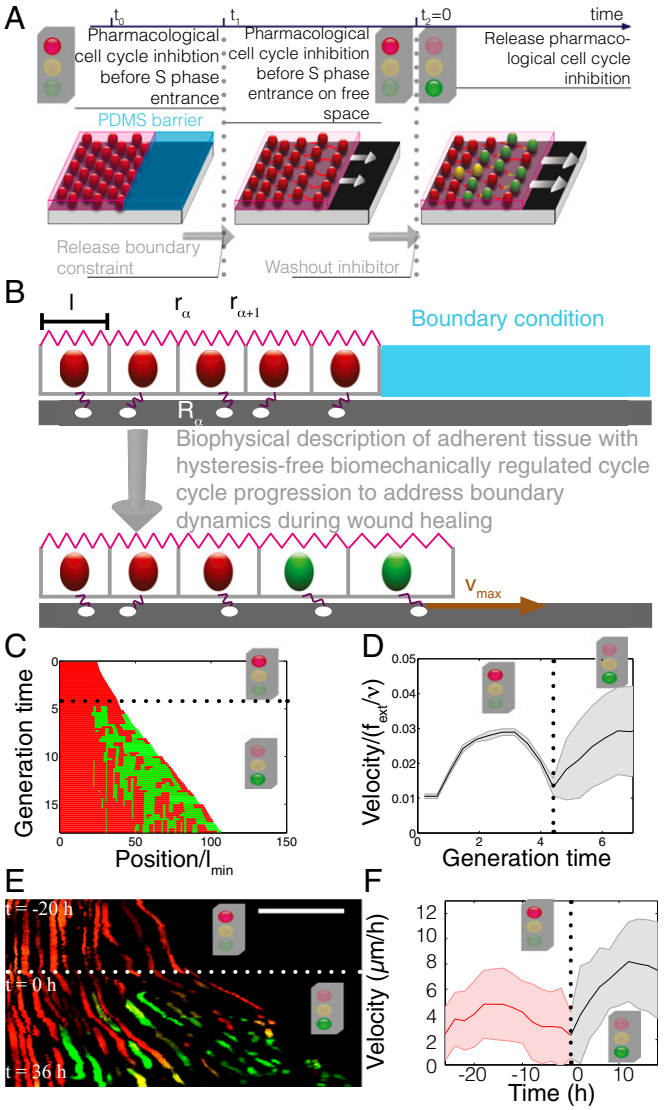

Fig. 4. Fast cell cycle activation after ERK signaling is reestablished, also far behind the leading edge. (*A*) Schematic of the tissue invasion assay. The cell cycle is blocked before S-phase entrance with MEK inhibitor, and the barrier is removed. Invasion of the free space and subsequent stalling of the tissue invasion in the absence of cell division are predicted by the model. (*B*) Biophysical tissue description. Vertices of cell α are labeled as $r_{\alpha+1}$ and r_α, respectively. Attachment points are shown as white dots, with the attachment point of cell α labeled as R_α. The boundary condition shown in the upper panel is removed upon the start of simulations, and a maximum traction force $f_{max} = \sigma v_{max}$ acts on the attachment point of the boundary cell. (*C*) Simulated tissue as a function of generation time and position. Color codes for cell cycle phase, except when S-phase entrance probability is forced to vanish for times above the black dotted line. (*D*) Boundary velocity of simulated tissues as in *C*. (*E*) Kymograph of the tissue colonization assay under MEK inhibitor. For negative control (DMSO only), see Fig S6. Washout at $t = 0$ h is indicated by the white dotted line. Scale bar: 100 μm. (*F*) Normal velocity of tissue boundary in the tissue colonization assay under cell cycle block. Time point $t = 0$ h corresponds to MEK inhibitor washout. Color codes are for active MEK inhibitor (red) or negative control (DMSO only, black). Error bar: SD.

(33–35). We propose that mechanical sensing of spatial constraints imposed by the environment may regulate the cell cycle of single cells and, by mechanical cell–cell coupling, also the proliferation rate within the entire tissue. In consequence, this provides a possible mechanism to prevent overcrowding, cell extrusion from the tissue, cell delamination, and apoptosis (16, 36, 37).

The kinetics of cell cycle adaptation allow us to speculate on the intracellular mechanism of sensing spatial constraints. The release of spatial constraints by substrate stretching led to rapid S-phase reentry within only 8 h (Fig. 2*E*). On the other hand, hysteresis-free adaption suggests a quasi-instantaneous control that acts independently of memory of prior constraints. Interestingly, we observed that this control acts on a timescale similar to that of Yes-associated protein (YAP) inactivation after inhibition of cytoskeletal tension (35, 38). Cytoskeletal tension therefore might serve as a mechanical read-out for spatial constraints to cell size and might be transduced to known regulators of growth, such as YAP, Skp2, or ERK (34, 35, 38–43). Although this system is faster than an average cell cycle, the 8-h delay in the proliferative response, together with the hysteresis-free adaption, would ensure that open space has to be available for a significant time to trigger an invasive response in a growing tissue and would prevent tissues from up-regulating cell proliferation in response to short-lived changes in their mechanical environment.

We found this cell cycle control mechanism in different model epithelia across species, suggesting that it is well conserved. Moreover, studies in vivo have provided evidence that such a mechanism might control cell proliferation in tissue development and disease (39, 44–47).

Our findings also provide a simple paradigm for the regulation of tissue regeneration. Here, cells would not require information on wound size, but simply would invade the site where space becomes available and where they experience consistently reduced mechanical constraints, subsequently activating movement and proliferation (26). Eventually, cell division fills the open space and thereby recreates the spatial constraints in the tissue, which reduces cell size until the FCC drops to steady-state levels. This provides a simple explanation for the regulation of cell proliferation during wound healing (2, 48).

We therefore propose that controlled tissue growth in many developmental and tumor invasion contexts is mediated by a mechanosensitive checkpoint that monitors spatial constraints to control cell cycle progression at the G1–S boundary.

Materials and Methods

All quantified experiments were performed at least in triplicate.

Cell Lines and Tissue Culture. MDCK-2 Fucci and mIMCD-3 Fucci cell lines were generated by infection of MDCK-2 and mIMCD-3 cells, respectively, with in-house–produced lentivirus coding for mAG-Geminin(1-110) and mKO2-Cdt1(30-120) (constructs were a gift from A. Miyawaki, Brain Science Institute, RIKEN, Wako-city, Japan). Virus production essentially followed the Trono laboratory protocols (http://tronolab.epfl.ch). Cell clones expressing both markers were sorted by FACS, and a clone of each cell type having unchanged morphology and cell cycle behavior, as well as a sufficient expression level of the transgenes, was selected by live cell imaging. MDCK-2 and mIMCD-3 cells were maintained in MEM (Sigma–Aldrich) supplemented with 9% (vol/vol) FBS or DMEM:F-12 (1:1) (Life Technologies) supplemented with 10% (vol/vol) FBS, respectively, at 37° C and 5% (vol/vol) CO_2. Cells on the stretcher device were seeded on strips of PDMS membrane coated with collagen I (Sigma–Aldrich) and imaged in a 37° C chamber with 85% (vol/vol) N_2, 10% (vol/vol) O_2, and 5% (vol/vol) CO_2.

Antibodies and Immunostaining. For immunostaining, cells were fixed with 4% (wt/vol) paraformaldehyde on the stretcher device, permeabilized with 0.2% Triton X-100, and stained for anti-E-cadherin (rr1; Developmental Studies Hybridoma Bank).

Tissue Invasion Assay. Cells were seeded in a glass-bottom culture dish (Willco Wells) that had half the glass surface covered by PDMS membrane. Cells were grown to contact inhibition in the empty half of the dish, and the PDMS barrier was removed, thereby releasing the boundary constraint for the tissue.

Stretching and Compression of Cells. Membranes were stretched to 50–120% of their original length while the position of the microscope stage was

readjusted continually to maintain the center of the field of view. Compression was performed likewise, and the membranes were relaxed by the indicated percentage of their length (i.e., from the stretched state).

MEK Inhibitor Treatment. MEK inhibitor U0126 (Promega) was dissolved in DMSO and used at a final concentration of 20 μM. Cells were pretreated with the inhibitor for ∼3 h before stretching or boundary release, respectively, and the inhibitor was renewed at most after 15 h. The negative controls (DMSO only) were treated according to the same protocol. For washout experiments, the medium was removed, the reservoir was washed once with imaging medium, and fresh medium was added.

Image Acquisition. Images were acquired with a UPlanApo 20×/N.A. 0.70 objective (Olympus Deutschland) and Andor iQ software (V1.10.5; Andor) at a customized confocal spinning-disk microscope with an automated stage (Märzhäuser Wetzlar), a spinning-disk unit (Yokogawa Europe), and an iXon3 897 EMCCD camera (Andor). For the boundary release and the stretching/compression experiments, z-stacks were acquired every 30 min and medium was exchanged every day. For the immunofluorescence staining, the stretcher device was mounted in PBS and z-stacks were acquired at a distance of 0.5 μm. For later montage construction, adjacent fields of view were imaged with an overlap of 10–20%.

Image Processing and Segmentation. Using a custom written image-processing routine in MATLAB, we first generated a maximum-intensity projection of each field of view (Fig. S2*A*) and then stitched the montage of the individual fields of view by using the Fourier transform phase correlation method (49) (Fig. S2*B*). This procedure resulted in a single stitched montage of the tissue for each time point. The resulting images were segmented using ILASTIK (50), and custom-written MATLAB routines were used to extract quantitative information on cell state and size. Nearest-neighbor point matching was used for cell tracking (see *SI Materials and Methods* for additional details).

ACKNOWLEDGMENTS. We thank A. Miyawaki for the kind gift of reagents. We are grateful to J. Ellenberg, D. Gilmour, R. Pepperkok, G. Bange, B. Shraiman, and all present and past members of the L.H. laboratory for helpful discussions. Furthermore, we are grateful to the European Molecular Biology Laboratory (EMBL) Flow Cytometry Core Facility for operating clonal sorting and for flow cytometric analysis of the Fucci cell lines, and to the EMBL Mechanical Workshop for building the stretcher device.

1. Thompson DW (1992) *On Growth and Form: The Complete Revised Edition* (Dover, New York).
2. Shaw TJ, Martin P (2009) Wound repair at a glance. *J Cell Sci* 122(Pt 18):3209–3213.
3. Jorgensen P, Tyers M (2004) How cells coordinate growth and division. *Curr Biol* 14(23):R1014–R1027.
4. Di Talia S, Skotheim JM, Bean JM, Siggia ED, Cross FR (2007) The effects of molecular noise and size control on variability in the budding yeast cell cycle. *Nature* 448(7156): 947–951.
5. Fantes P, Nurse P (1977) Control of cell size at division in fission yeast by a growth-modulated size control over nuclear division. *Exp Cell Res* 107(2):377–386.
6. Killander D, Zetterberg A (1965) Quantitative cytochemical studies on interphase growth. I. Determination of DNA, RNA and mass content of age determined mouse fibroblasts in vitro and of intercellular variation in generation time. *Exp Cell Res* 38: 272–284.
7. Conlon I, Raff M (2003) Differences in the way a mammalian cell and yeast cells coordinate cell growth and cell-cycle progression. *J Biol* 2(1):7.
8. Dolznig H, Grebien F, Sauer T, Beug H, Müllner EW (2004) Evidence for a size-sensing mechanism in animal cells. *Nat Cell Biol* 6(9):899–905.
9. Echave P, Conlon IJ, Lloyd AC (2007) Cell size regulation in mammalian cells. *Cell Cycle* 6(2):218–224.
10. Tzur A, Kafri R, LeBleu VS, Lahav G, Kirschner MW (2009) Cell growth and size homeostasis in proliferating animal cells. *Science* 325(5937):167–171.
11. Son S, et al. (2012) Direct observation of mammalian cell growth and size regulation. *Nat Methods* 9(9):910–912.
12. Bryant DM, Mostov KE (2008) From cells to organs: Building polarized tissue. *Nat Rev Mol Cell Biol* 9(11):887–901.
13. Lecuit T, Lenne PF (2007) Cell surface mechanics and the control of cell shape, tissue patterns and morphogenesis. *Nat Rev Mol Cell Biol* 8(8):633–644.
14. Friedl P, Wolf K (2003) Tumour-cell invasion and migration: Diversity and escape mechanisms. *Nat Rev Cancer* 3(5):362–374.
15. Folkman J, Moscona A (1978) Role of cell shape in growth control. *Nature* 273(5661): 345–349.
16. Chen CS, Mrksich M, Huang S, Whitesides GM, Ingber DE (1997) Geometric control of cell life and death. *Science* 276(5317):1425–1428.
17. Nelson CM, et al. (2005) Emergent patterns of growth controlled by multicellular form and mechanics. *Proc Natl Acad Sci USA* 102(33):11594–11599.
18. Shraiman BI (2005) Mechanical feedback as a possible regulator of tissue growth. *Proc Natl Acad Sci USA* 102(9):3318–3323.
19. Abercrombie M (1970) Contact inhibition in tissue culture. *In Vitro* 6(2):128–142.
20. Puliafito A, et al. (2012) Collective and single cell behavior in epithelial contact inhibition. *Proc Natl Acad Sci USA* 109(3):739–744.
21. Wilson E, Mai Q, Sudhir K, Weiss RH, Ives HE (1993) Mechanical strain induces growth of vascular smooth muscle cells via autocrine action of PDGF. *J Cell Biol* 123(3): 741–747.
22. Sudhir K, Wilson E, Chatterjee K, Ives HE (1993) Mechanical strain and collagen potentiate mitogenic activity of angiotensin II in rat vascular smooth muscle cells. *J Clin Invest* 92(6):3003–3007.
23. Kaspar D, Seidl W, Neidlinger-Wilke C, Claes L (2000) In vitro effects of dynamic strain on the proliferative and metabolic activity of human osteoblasts. *J Musculoskelet Neuronal Interact* 1(2):161–164.
24. Miller CE, Donlon KJ, Toia L, Wong CL, Chess PR (2000) Cyclic strain induces proliferation of cultured embryonic heart cells. *In Vitro Cell Dev Biol Anim* 36(10): 633–639.
25. Liu WF, Nelson CM, Tan JL, Chen CS (2007) Cadherins, RhoA, and Rac1 are differentially required for stretch-mediated proliferation in endothelial versus smooth muscle cells. *Circ Res* 101(5):e44–e52.
26. Nikolić DL, Boettiger AN, Bar-Sagi D, Carbeck JD, Shvartsman SY (2006) Role of boundary conditions in an experimental model of epithelial wound healing. *Am J Physiol Cell Physiol* 291(1):C68–C75.
27. Poujade M, et al. (2007) Collective migration of an epithelial monolayer in response to a model wound. *Proc Natl Acad Sci USA* 104(41):15988–15993.
28. Sakaue-Sawano A, et al. (2008) Visualizing spatiotemporal dynamics of multicellular cell-cycle progression. *Cell* 132(3):487–498.
29. Vitorino P, Meyer T (2008) Modular control of endothelial sheet migration. *Genes Dev* 22(23):3268–3281.
30. Smith JA, Martin L (1973) Do cells cycle? *Proc Natl Acad Sci USA* 70(4):1263–1267.
31. Farhadifar R, Röper JC, Aigouy B, Eaton S, Jülicher F (2007) The influence of cell mechanics, cell-cell interactions, and proliferation on epithelial packing. *Curr Biol* 17(24):2095–2104.
32. Hufnagel L, Teleman AA, Rouault H, Cohen SM, Shraiman BI (2007) On the mechanism of wing size determination in fly development. *Proc Natl Acad Sci USA* 104(10): 3835–3840.
33. Vogel V, Sheetz M (2006) Local force and geometry sensing regulate cell functions. *Nat Rev Mol Cell Biol* 7(4):265–275.
34. Paszek MJ, et al. (2005) Tensional homeostasis and the malignant phenotype. *Cancer Cell* 8(3):241–254.
35. Dupont S, et al. (2011) Role of YAP/TAZ in mechanotransduction. *Nature* 474(7350): 179–183.
36. Eisenhoffer GT, et al. (2012) Crowding induces live cell extrusion to maintain homeostatic cell numbers in epithelia. *Nature* 484(7395):546–549.
37. Marinari E, et al. (2012) Live-cell delamination counterbalances epithelial growth to limit tissue overcrowding. *Nature* 484(7395):542–545.
38. Aragona M, et al. (2013) A mechanical checkpoint controls multicellular growth through YAP/TAZ regulation by actin-processing factors. *Cell* 154(5):1047–1059.
39. Jiang X, et al. (2009) Mechanoregulation of proliferation. *Mol Cell Biol* 29(18): 5104–5114.
40. Birukov KG, et al. (1997) Increased pressure induces sustained protein kinase C-independent herbimycin A-sensitive activation of extracellular signal-related kinase 1/2 in the rabbit aorta in organ culture. *Circ Res* 81(6):895–903.
41. Reusch HP, Chan G, Ives HE, Nemenoff RA (1997) Activation of JNK/SAPK and ERK by mechanical strain in vascular smooth muscle cells depends on extracellular matrix composition. *Biochem Biophys Res Commun* 237(2):239–244.
42. Numaguchi K, Eguchi S, Yamakawa T, Motley ED, Inagami T (1999) Mechanotransduction of rat aortic vascular smooth muscle cells requires RhoA and intact actin filaments. *Circ Res* 85(1):5–11.
43. Sawada Y, et al. (2001) Rap1 is involved in cell stretching modulation of p38 but not ERK or JNK MAP kinase. *J Cell Sci* 114(Pt 6):1221–1227.
44. Pyles JM, et al. (1997) Activation of MAP kinase in vivo follows balloon overstretch injury of porcine coronary and carotid arteries. *Circ Res* 81(6):904–910.
45. Thubrikar MJ, Robicsek F (1995) Pressure-induced arterial wall stress and atherosclerosis. *Ann Thorac Surg* 59(6):1594–1603.
46. Yamazaki T, Komuro I, Shiojima I, Yazaki Y (1999) The molecular mechanism of cardiac hypertrophy and failure. *Ann N Y Acad Sci* 874:38–48.
47. Hahn C, Schwartz MA (2009) Mechanotransduction in vascular physiology and atherogenesis. *Nat Rev Mol Cell Biol* 10(1):53–62.
48. Cooper L, Johnson C, Burslem F, Martin P (2005) Wound healing and inflammation genes revealed by array analysis of 'macrophageless' PU.1 null mice. *Genome Biol* 6(1):R5.
49. Kuglin CD, Hines DC (1975) The phase correlation image alignment method. *Proceedings of IEEE International Conference on Cybernetics and Society* (IEEE, New York), pp 163–165.
50. Sommer C, Straehle C, Koethe U, Hamprecht FA (2011) Ilastik: Interactive learning and segmentation toolkit. *Eighth IEEE International Symposium on Biomedical Imaging* (IEEE, Chicago), pp 230–233.